Case Report

Discovery Medicine 2025; 37(197): 1130–1138
https://doi.org/10.24976/Discov.Med.202537197.100

Computed Tomography Imaging for the Diagnosis of Primary Sarcomatoid Carcinoma of the Lung: A Case Report

Li-Feng Xu[1], Xi-Sheng Zhou[1], Feng Chen[1], Ping Zhu[2,*]

[1]Department of Radiology, Tong Xiang First People's Hospital, 314500 Tongxiang, Zhejiang, China
[2]Department of Radiology, The Second Affiliated Hospital of Zhejiang Chinese Medical University, 310005 Hangzhou, Zhejiang, China
*Correspondence: zhupinghz@zcmu.edu.cn (Ping Zhu)
Published: 9 June 2025

Aim: Primary sarcomatoid carcinoma (PSC) of the lung is a rare malignant neoplasm characterized by the presence of both carcinomatous and sarcomatoid components, typically presenting as a solitary pulmonary mass. Imaging examination serves as a critical tool for the detection and evaluation of pulmonary lesions, the definitive diagnosis of PSC still relies on histopathological examination and immunohistochemical staining results. This study presents a pathologically confirmed case of PSC of the lung with a retrospective analysis of the clinical features and chest computed tomography (CT) imaging findings. The purpose is to improve the diagnostic accuracy of this disease.

Case Presentation: A 67-year-old Chinese male was admitted to the First People's Hospital of Tong Xiang City with a one-week history of cough and expectoration. A plain and contrast-enhanced chest CT scan revealed a large mass in the upper lobe of the right lung, adjacent to the interlobar fissure and parietal pleura. Upon enhancement, the mass demonstrated irregular mild-to-moderate enhancement on the side near the pleura, with no significant enhancement in the central region or near the hilum. A pseudocapsule was observed surrounding the lesion. The patient subsequently underwent resection of the right upper lobe mass. Hematoxylin-eosin staining of the pathological specimen revealed spindle-shaped tumor cells that had invaded the parietal pleura. Immunohistochemical analysis showed positivity for vimentin and cytokeratin, as well as partial positivity for epithelial membrane antigen. Based on these immunohistochemical findings, the tumor was diagnosed as pulmonary sarcomatoid carcinoma (spindle cell type). Approximately 10 months postoperatively, the patient was readmitted due to chest pain and dyspnea lasting four days. The chest CT scan indicated tumor recurrence. The patient was managed conservatively for two months, achieving stable condition before discharge. Two months after discharge, the patient succumbed to complications of concurrent pulmonary infection and cardiopulmonary failure.

Results: Analyzing the pathological findings and CT manifestations in a patient with pulmonary PSC; immunohistochemical staining results can to some extent provide insights into the patient's prognosis.

Conclusions: Owing to the rarity, high-degree malignancy and poor prognosis of PSC, potential cases should be comprehensively evaluated based on imaging, laboratory and pathological results. Long-term regular follow-up is required to rule out the metastasis or recurrence of postoperative pleural metastasis.

Keywords: primary sarcomatoid carcinoma; malignant tumor; imaging findings; computed tomography

Introduction

Pulmonary sarcomatoid carcinoma (PSC) is a rare malignant tumor composed of both carcinomatous and sarcomatous components, accounting for 0.3%–4.7% of non-small cell lung cancers (NSCLC) and 0.1%–0.4% of all pulmonary malignancies [1]. PSC is characterized by aggressive behavior, high metastatic potential, poor prognosis, and elevated recurrence rates [2], underscoring the importance of early clinical detection and diagnosis. Imaging examinations play a pivotal role in this process, particularly with the advancement of multi-slice spiral computed tomography (MSCT), whose improved spatial resolution and postprocessing capabilities have enabled more comprehensive evaluation of morphological features and peritumoral tissue relationships [3]. In this report, we present a case of PSC with retrospective analysis of its clinical characteristics and imaging findings, supplemented by a literature review to enhance the understanding of this disease entity.

Materials and Methods

CT Image Acquisition and Post-Processing

The imaging examination was performed using 16-slice spiral CT scanner (Philips Brilliance, Holland). The patient was placed in the supine position with both arms

raised above the head. Scanning was conducted from the thoracic inlet to the base of the lungs. A dual-chamber high-pressure injector (Medrad Stellant D-CE, Germany) was used to administer 100 mL of iopromide (Ultravist 370, non-ionic contrast agent, Bayer AG, Germany) via the antecubital vein at a rate of 4.0 mL/s, followed by 20 mL of normal saline. Scanning parameters were set as follows: The scanning parameters included a collimation width of 16 mm × 0.75 mm, tube voltage of 120 kV, tube current of 420 mA, and a pitch of 1.5. The matrix size was 512 × 512, with reconstructed slice thickness and interval both set at 5 mm. Raw image data were transferred to a Philips EBW 4.0 workstation for image analysis using postprocessing techniques, including multiplanar reconstruction and volume rendering.

Immunohistochemical Staining

Immunohistochemical staining was performed using the EnVision System (Dako, USA) on the Autostainer Link 48 automated staining platform (Agilent, USA). The collected tissue samples were subjected to processing prior to immunohistochemical staining. Tissue samples were decalcified using Ethylenediaminetetraacetic acid (EDTA) decalcification solution (Cida Biotechnology Co., Ltd., China), followed by gradient dehydration with a LEiCA TP-1020 dehydrator. After paraffin embedding, 4–5 µm sections were prepared using a LEiCA HistoCore MULTICUT microtome. Sections were flattened with a tissue spreader and baked at 60 °C for 30–60 minutes to ensure tissue adhesion. Primary antibodies (DAKO ready-to-use, undiluted) utilized in the immunohistochemical staining include: anti-Vimentin (clone number V9, product number IR630); anti-Cytokeratin (CK) (clone number AE1/AE3, product number IR053); anti- Epithelial Membrane Antigen (EMA) (clone number E29, product number IR629), anti-calretinin (clone number DAK-calret 1, product number IR627); anti-CD3 (clone number F7.2.38, product number IR503); anti-CD20 (clone number L26, product number IR604); anti-S-100 (clone number GA504, product number GA504); anti-Melanosome (clone number HMB-45, product number IR052); anti-Thyroid Transcription Factor (TTF)-1 (clone number 8G7G3/1, product number IR056); anti-P63 (clone number DAK-P63, product number IR662); anti-Podoplanin (clone number D2-40, product number IR072); anti-Smooth Muscle Actin (SMA) (clone number IA4, product number IR611); anti-Ki-67 (clone number MIB-1, product number IR626); and anti-melan-A (clone number A103, product number IR633). Secondary antibodies: Horseradish Peroxidase (HRP)-labeled goat anti-rabbit IgG(H+L) antibody (DAKO, number: K8002) was used at a dilution of 1:800, and DAKO EnVision FLEX+ (Mouse, High pH, LINK) ready-to-use Peroxidase (POD)-labeled polymer.

At the beginning of the immunohistochemical staining, the tissue samples were subjected to deparaffinization through a gradient of xylene and hydration through ethanol gradient. Then, the samples were incubated with 3% H_2O_2-methanol solution for 20 minutes at room temperature to achieve endogenous peroxidase blocking. Depending on target protein requirements, antigen retrieval was performed by means of high-temperature heat-induced epitope retrieval or enzymatic retrieval; in certain cases, no retrieval was required. Subsequently, the tissue samples were separately incubated with primary antibody at 37 °C for 30–60 minutes, or alternatively, at room temperature for 1 hour or at 4 °C overnight. This was followed by secondary antibody incubation using EnVision FLEX+ polymer at 37 °C (or room temperature) for 20–30 minutes. Diaminobenzidine (DAB) chromogenic reaction was initiated for 3–10 minutes, followed by hematoxylin counterstaining for 1–2 minutes. The samples were observed using a microscope. Acidic ethanol differentiation was performed on the samples for a few seconds, followed by 5-minute bluing under running water. Eventually, the samples were subjected to dehydration through a gradient of ethanol and xylene clearing, prior to mounting with neutral resin.

Hematoxylin-Eosin Staining

Hematoxylin-eosin (H&E) staining was performed using reagents from Ningbo Tongsheng Biotechnology Co., Ltd. (China), specifically encompassing H&E High-Definition Alcohol-Soluble Eosin Staining Solution (Lot No. 170914911) and H&E High-Definition Hematoxylin Staining Solution (Lot No. 170915414). The staining procedure is as follows: (1) The tissue sections were first baked at 60 °C for 30–60 minutes to enhance adhesion. (2) Deparaffinization was then conducted by immersing the tissue samples in xylene (I) and (II) for 5–10 minutes each. (3) The tissue sections were subjected to gradient hydration, starting from absolute ethanol for 1–5 minutes, followed by 95% ethanol for 1–5 minutes, 75% ethanol for 1–5 minutes, and water rinsing. (4) Hematoxylin staining was conducted by immersing the sections in the reagent solution for 5–20 minutes. Afterwards, they were rinsed with water and evaluated microscopically to confirm optimal nuclear staining. (5) Subsequently, the sections were treated with 1% hydrochloric acid ethanol for seconds, followed by a water rinse and a microscopic re-evaluation. (6) This was followed by bluing, which was performed with a 5-minute rinsing under running water. (7) Eosin counterstaining: Stain for several seconds, then rinse with 75%–85% ethanol for 30 seconds after cytoplasmic coloration. (8) The sections were then subjected to gradient dehydration using 95% ethanol (I, 0.5–2 minutes; II, 2–5 minutes) and absolute ethanol (I and II, 2–5 minutes each). (9) Eventually, the tissue sections were cleared using xylene (I and II, 1 minute each) and mounted with neutral resin. Typically, nuclei should be stained blue with hematoxylin and cytoplasm stained pink with eosin. Stained sections were observed using an OLYMPUS CKX43-LP microscope and

digitally panormscopic imaging was performed through the 3DHISTECH P250FLASH panoramic scanner.

Laboratory Examination

Following the collection of venous blood samples from patients, centrifugation separation was performed at 3000–3500 rpm for 10 minutes. The separated serum/plasma was subsequently aliquoted into secondary tubes, which were then kept for long term in the freezer to avoid repeated freeze-thaw cycles. Complete blood count (CBC) analysis was conducted using the Mindray CL8000 automated hematology analyzer. Serum tumor biomarker detection was performed through chemiluminescence immunoassay (CLIA) technology employing the Beckman Dxl800 and YHLO iFlash 3000-C chemiluminescence analysis systems. All testing procedures were executed in strict compliance with standardized operating protocols of the instruments utilized, with rigorous implementation of calibration protocols and quality control measures throughout the analytical process.

Results

A 67-year-old Chinese male patient was admitted to the First People's Hospital of Tong Xiang City on 20 February 2017, following the detection of a space-occupying lesion in the right lung during a routine physical examination via chest CT. The patient reported symptoms of cough and sputum production. He denied any history of residence in areas endemic for tuberculosis or influenza, contact with individuals from such regions, as well as a history of smoking or alcohol consumption. This case report was conducted in compliance with the Declaration of Helsinki (2013). The protocol of this study was approved by the hospital's Ethics Review Committee (Approval No. 2024-208). The present case report was prepared according to the CARE (Case Report) guidelines, and the completed CARE checklist is included in the **Supplementary Material**.

Complete blood count analysis revealed a markedly elevated white blood cell count of 15.8 $\times$ 10^9/L (reference: 4–10 $\times$ 10^9/L), decreased lymphocyte percentage (11.2%, reference: 20%–40%), elevated neutrophil percentage (74.6%, reference: 50%–70%), and increased eosinophil percentage (8.8%, reference: 0.5%–5%). Serum tumor biomarker profiles demonstrated that: pro-gastrin-releasing peptide (ProGRP) = 39.6 pg/mL (reference: $<$68.3 pg/mL); squamous cell carcinoma antigen (SCC) = 0.97 ng/mL (reference: 0.00–1.81); cytokeratin 19 fragment = 2.7 ng/mL (reference: 0.0–3.3); neuron-specific enolase (NSE) = 9.9 ng/mL (reference: 0.0–16.3); and carcinoembryonic antigen (CEA) = 2.88 ng/mL (reference: 0.00–5.00). All levels of these tumor markers remained within normal reference ranges.

A plain and contrast-enhanced chest CT scan revealed a mass shadow approximately 5.8 cm $\times$ 5.2 cm $\times$ 5.0 cm in size located in the upper lobe of the right lung. The lesion was closely adherent to the interlobar fissure and lateral pleura, with well-defined margins but heterogeneous internal density. The CT value ranged from 7 to 40 HU. The density near the hilum was relatively low, and no obvious abnormalities were detected in the surrounding lung tissue (Fig. 1A,B). On contrast-enhanced CT, the average CT values for the mass near the pleural side were 40 HU on plain scan, 48 HU in the arterial phase, and 52 HU in the venous phase, indicating irregular mild to moderate enhancement. The central area showed no significant enhancement, particularly on the hilar side, where the average CT value was approximately 15 HU. A pseudocapsule was observed around the periphery (Fig. 1C–F), and no enlarged lymph nodes were identified in either hilar or mediastinal regions. The diagnosis suggested a pulmonary neoplastic lesion, with benign or malignant nature requiring confirmation via biopsy. Brain metastases were ruled out by plain and contrast-enhanced cranial magnetic resonance imaging (MRI), which demonstrated no abnormal findings.

On 24 February 2017, the patient underwent thoracoscopic resection of the right upper lung mass and lymphadenectomy under general anesthesia. During surgery, significant adhesion between the right upper lung and the chest wall was noted. Pathological exploration confirmed a mass with a firm texture in the right upper lung, measuring approximately 6 cm in diameter. Non-invasive oval forceps were used to clamp and fix the mass, and lung tissue was clamped approximately 1 cm away from the lesion. The mass was resected in a wedge shape using an endoscopic stapler, and the specimen was removed. Lymph nodes in stations 7, 8, 10, and 11 were dissected. The procedure proceeded smoothly. After hemostasis was achieved, the right thoracic cavity was irrigated with warm water, and a drainage tube was placed at the seventh intercostal space along the mid-axillary line. No active bleeding was observed in the thoracic cavity, and the chest was routinely closed.

According to the pathological and immunohistochemical findings on 10 March 2017, the resected specimen of the right upper lung mass, measuring 7.0 cm $\times$ 5.0 cm $\times$ 3.5 cm in size, was found invading the parietal pleura. H&E staining revealed spindle-shaped tumor cells that had infiltrated the parietal pleura, with negative surgical margins at the lung suture site (Fig. 2A). Emphysema was noted in the surrounding lung tissue. No cancer metastasis was detected in the examined lymph nodes. Immunohistochemical staining results are as follows: vimentin—positive (Fig. 2B), CK—positive (Fig. 2C), EMA—partially positive (Fig. 2D), CK7—partially positive (Fig. 2F), CK20—negative, CD20—negative, CD3—negative, S-100—negative, Human melanoma black (HMB) 45—negative, TTF-1—positive (Fig. 2E), P63—negative, D2-40—negative, calretinin—negative, Ki67—40% positive (Fig. 2G), SMA—negative, and

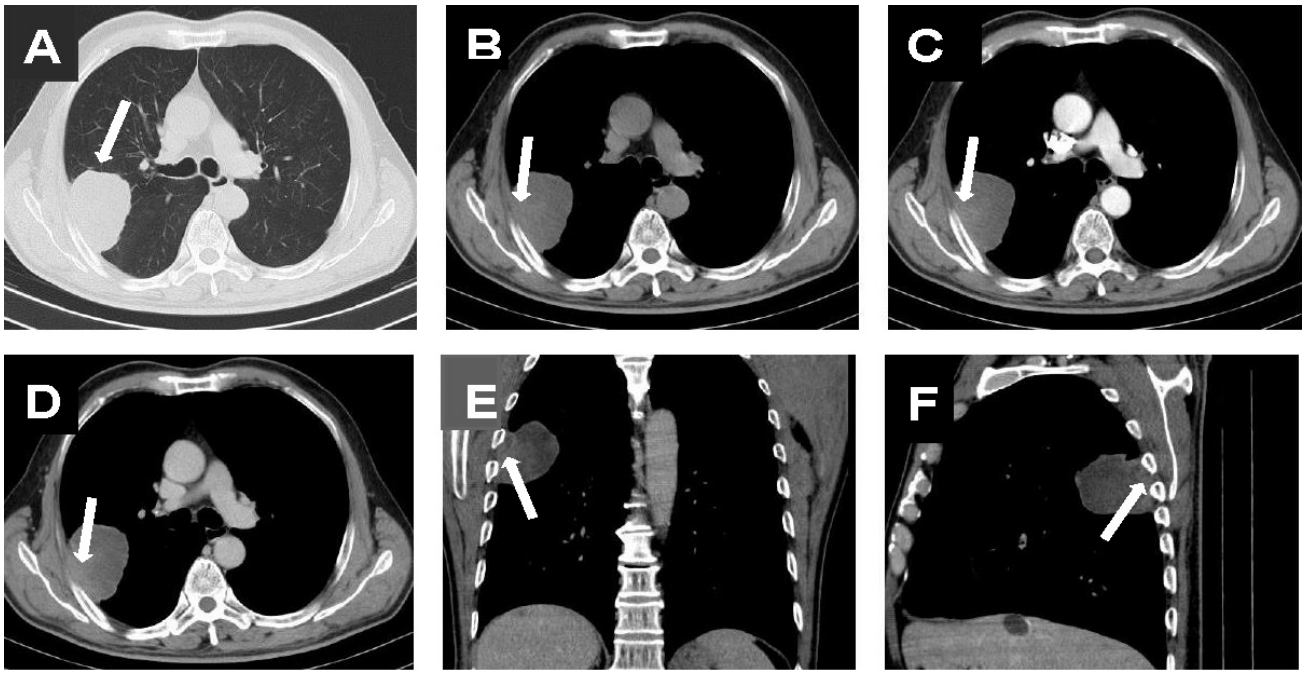

Fig. 1. Preoperative chest computed tomography (CT) plain scan and contrast-enhanced examination. (A) Pulmonary window of the chest CT scan shows that the lesion is located in the upper lobe of the right lung (arrow), abutting the interlobar fissure and the parietal pleura. (B) Mediastinal window of the chest CT scan suggests a well-defined margin and heterogeneous internal density of the mass (arrow), ranging from 7 to 40 HU on CT value, the density was lower near the hilum, with no significant abnormalities observed in the surrounding pulmonary tissue. (C–F) Contrast-enhanced scanning showed irregular mild to moderate enhancement of the mass near the pleura, with no significant enhancements in the central area and near the hilum. There is a pseudocapsule around the lesion (arrows).

melan-A—partially positive (Fig. 2H). Based on these findings, the characteristics of this lesion were consistent with those of PSC (spindle cell carcinoma). During hospitalization, the patient received continuous symptomatic treatments, including anti-infection therapy and fluid infusion, with good control of the condition. One week later, the patient was discharged.

Approximately 10 months postoperatively, on 25 December 2017, the patient was readmitted due to sudden onset of chest pain and dyspnea lasting 4 days, accompanied by cough, expectoration, and nocturnal paroxysmal dyspnea. Physical examination revealed a palpable mass on the right chest wall. A plain chest CT scan demonstrated a large soft tissue mass in the surgical area of the right lung, measuring approximately 5.7 cm $\times$ 7.9 cm, with heterogeneous density and infiltration into the chest wall. Local patchy high-density shadows were also observed (Fig. 3A,B). Right-sided pleural effusion was present, with partial encapsulation causing incomplete compression and dilation of the lower lobe of the right lung (Fig. 3C,D).

Postoperative tumor recurrence and chest wall invasion with local hemorrhage were suspected. A pathological fracture of the fourth rib on the right side was also noted. Laboratory findings included markedly elevated white blood cell count (48.6 $\times$ 10^9/L, reference: 4–10 $\times$ 10^9/L), decreased hemoglobin (88 g/L, reference: 115–150 g/L), and elevated neutrophil count (37.4 $\times$ 10^9/L, reference: 2–7 $\times$ 10^9/L). Upon admission, conventional anti-infection treatment, fluid replacement, potassium supplementation, and other conservative measures were initiated. On 5 January 2018, it was determined that the patient's condition had deteriorated, with potential for further tumor progression. Following thorough discussions with the patient's family, targeted anti-tumor therapy with apatinib was administered in two courses. The drug (National Drug Approval No. H20140103), manufactured by Jiangsu Hengrui Pharmaceuticals Co., Ltd. (China), was administered orally at a daily dose of one tablet (0.425 g/tablet). To alleviate cough and chest tightness, closed thoracic drainage was performed between the second and third ribs along the midclavicular line on 1 February 2018, resulting in the removal of 200 mL of purulent and bloody fluid. On 21 February 2018, the patient was discharged after having achieved stabilization. Approximately 2 months later, the patient succumbed to concurrent pulmonary infection and cardiopulmonary failure.

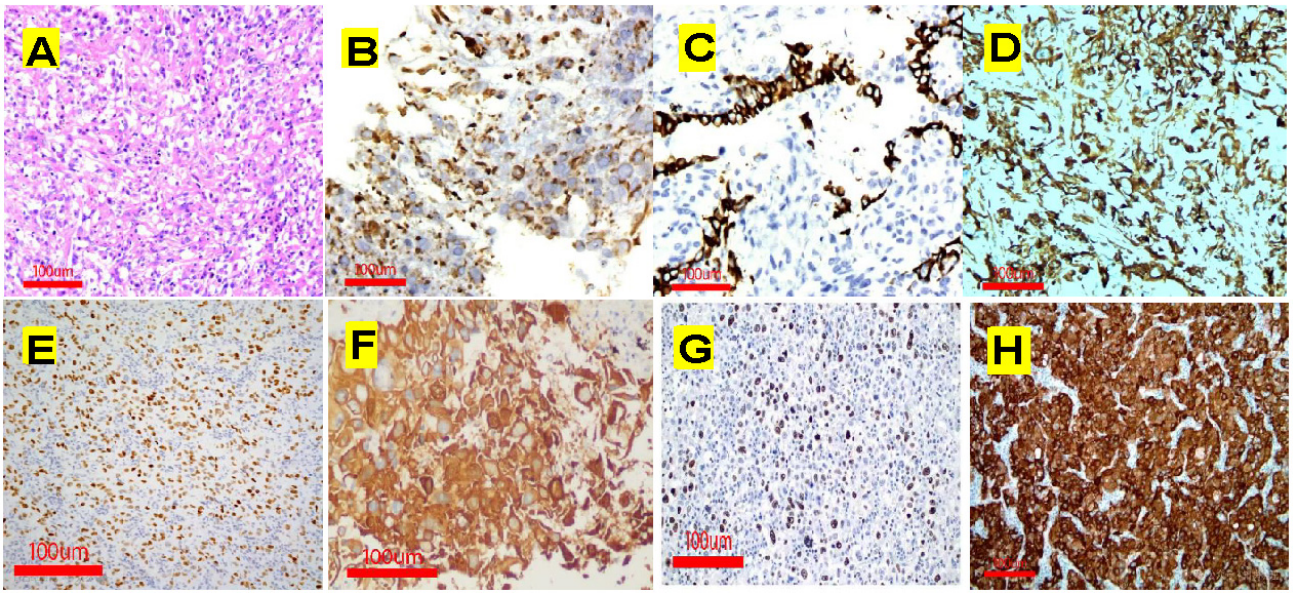

Fig. 2. The pathological and immunohistochemical results of right upper lung mass (scale bar: 3 µm). (A) Slice specimens stained with hematoxylin-eosin (H&E) demonstrate arrangement of tumor cells in fusiform shapes. (B–H) Immunohistochemical staining results are as follows: (B) Vimentin was positive (EnVision two step method). (C) Cytokeratin (CK) was positive (EnVision two-step method, double staining with elastic fiber). (D) Epithelial antigen (EMA) was positive (cell membrane-specific staining, EnVision two-step method). (E) Thyroid Transcription Factor (TTF)-1 was positive. (F) CK7 was positive. (G) Ki67 was positive. (H) Melan-A was positive.

Discussion

Clinical Manifestations and Pathological Features of PSC

PSC is a rare tumor characterized by high degree of malignancy and heterogeneity. It is a biphasic neoplasm composed of epithelial and mesenchymal tissues, exhibiting both epithelial and mesenchymal features. Compared with other NSCLCs, PSC demonstrates significantly worse overall survival rates and prognoses [4]. The prevalence is higher among elderly males, heavy smokers, and individuals exposed to dust, chemicals, or radiation for prolonged periods. Research conducted by Mansfield *et al*. [5] highlights that smoking plays a critical role in the pathogenesis and prognosis of PSC. The most common site of occurrence for PSC is the right lung, particularly the upper lobe of the right lung, while the exact reason remains unclear [6]. Clinically, PSC presents symptoms similar to those of other NSCLCs; this explains why its symptoms lack specificity. Common manifestations include cough, sputum production, hemoptysis, and dyspnea. Pleural or chest wall involvement may result in chest pain. PSC exhibits high invasiveness, with lymph node metastasis and hematogenous dissemination occurring at an early stage [7]. According to a study utilizing the National Cancer Database (NCDB) [8], the median survival period for PSC patients (6.4 months) was approximately half that of other NSCLC patients, with this survival disparity being statistically significant across all stages. The current case features an elderly male with a solitary mass in the upper lobe of the right lung, who denied history of smoking and exhibited symptoms of cough and sputum production. Cranial MRI revealed no evidence of brain metastases. These findings were consistent with prior reports.

In the 2021 WHO classification, PSC is subdivided into five subtypes: pleomorphic carcinoma (PC), SCC, giant cell carcinoma (GCC), carcinosarcoma (CS), and pulmonary blastoma (PB) [9]. PC refers to a tumor comprising poorly differentiated non-small cell carcinomas (squamous cell carcinoma, adenocarcinoma, or large cell carcinoma) with at least 10% spindle cell and/or giant cell components. SCC consists entirely of spindle-shaped tumor cells, while GCC involves a non-small cell carcinoma composed exclusively of pleomorphic tumor giant cells. CS represents a mixed malignant tumor incorporating cancer and differentiated sarcoma components (e.g., malignant cartilage, bone, or striated muscle). Among these, PC, SCC, and GCC account for approximately 90% of all PSC cases, whereas CS and PB are rare [10]. Immunohistochemical analysis reveals that PSC exhibits characteristics of both cancer and sarcoma components, with positive expression of epithelial markers such as CK, EMA, and AE1/AE3, as well as mesenchymal markers like vimentin and desmin. Simultaneous positive expression of CK and vimentin is a hallmark pathological feature of PSC [11]. Melan-A protein, a melanocyte differentiation antigen, is typically considered a specific

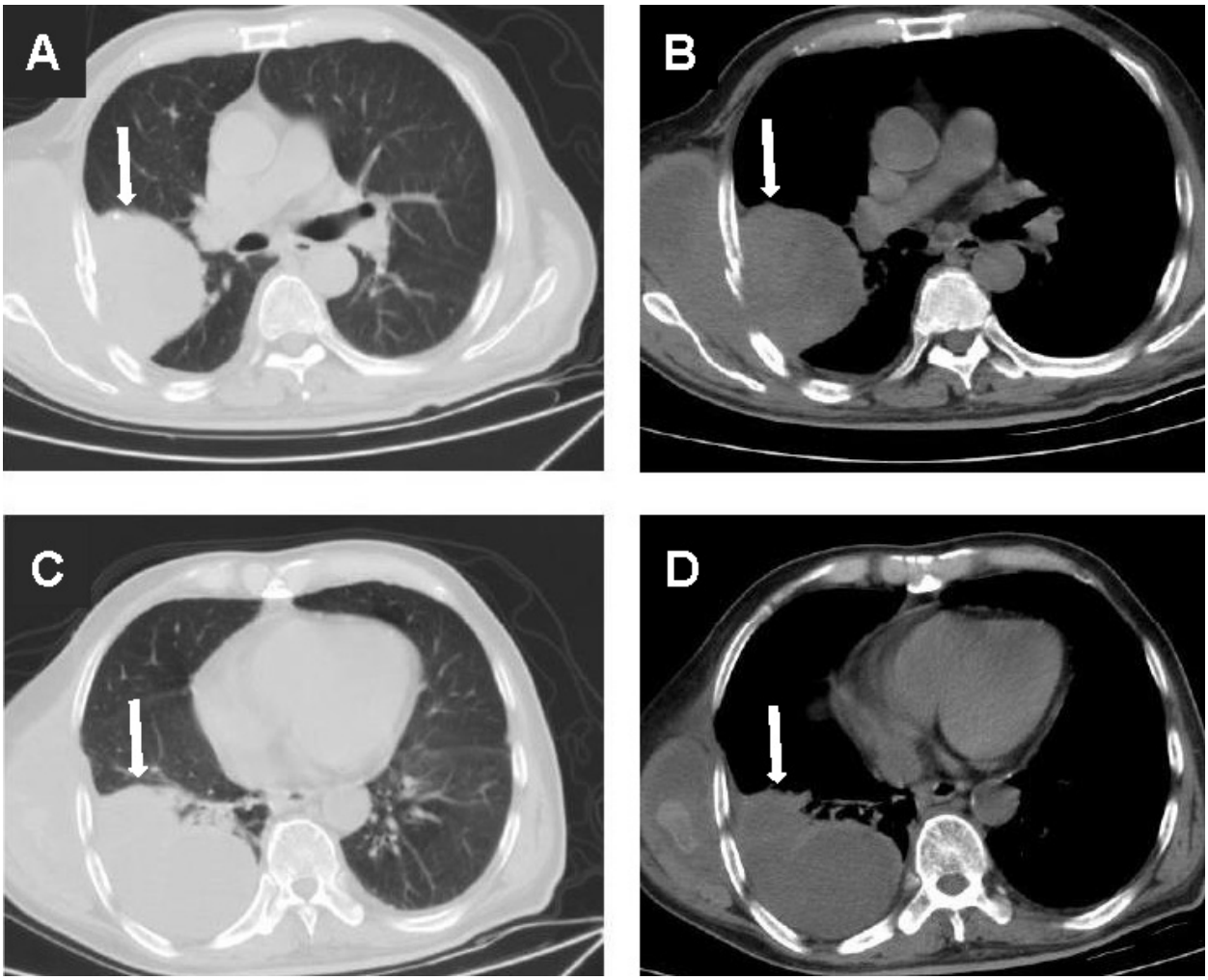

Fig. 3. Chest CT plain scan 10 months postoperatively. (A,C) A huge soft tissue mass (indicated by arrows) could be seen at the right lung surgery area. (B,D) The mass density wasuneven, with a local patchy high-density shadow and infiltrates the chest wall (indicated by arrows).

marker of melanocytes. A study has reported that out of six cases of non-melanoma tumors expressing melan-A, five cases showed weak positivity and the remaining one diffuse strong positivity [12]. All cases demonstrated positive CK expression, with CK7 and EMA positively expressed in two pulmonary cases. Among the six cases, five exhibited distant metastasis, and four patients had succumbed to the disease at the time of writing. These findings suggest that melan-A positivity is significantly associated with poorer survival rates and may serve as a potential marker of poor prognosis in non-melanoma tumors. Ki-67, although not independently predictive in multivariate analyses, reflects low survival rates and high invasiveness due to its high proliferation rate in malignant tumors. A study on the prognostic value of the Ki-67 labeling index for NSCLC identified significant variability in Ki-67 expression levels, with critical thresholds ranging from 5% to 30% used to differentiate high and low proliferation rates [13]. Some studies indicated that a high Ki-67 expression was a statistically significant negative prognostic factor for overall survival or disease-free survival in NSCLC, though differences in its prognostic impact across various histological subtypes remain unconfirmed. Immunohistochemical staining of this patient revealed positive expression of epithelial and mesenchymal markers, including CK and vimentin. H&E staining of postoperative pathological specimens confirmed a spindle-shaped arrangement of tumor cells, identifying the SCC subtype of PSC. Notably, varying expression rates of CK7 (+ve), EMA (partially +ve), melan-A (partially +ve), and Ki-67 (>40% +ve) suggested highly aggressive biological behavior of the tumor and a tendency toward poor prognosis. Approximately 10 months postoperatively, the tumor recurred. Pathological results indicated parietal pleural invasion, suggesting visceral pleural breach and infiltration into the pleural cavity, which increased the risk of local dissemination. Negative surgical margins, despite recurrence, may indicate the presence of micrometastases or circulating tumor cells undetectable by conventional approaches dur-

ing surgery. Collectively, these histopathological and immunohistochemical findings during surgery suggest a potentially poor clinical prognosis for the patient.

CT Manifestations of PSC

The imaging manifestations of the various subtypes of PSC exhibit minimal differences. The primary findings include circular or oval solid mass shadows within the lungs. These lesions are typically large, often exceeding 3.0 cm in diameter, and possess well-defined and smooth margins. Lobulation may be observed but spiculation is relatively uncommon. Due to their substantial size, necrosis and hemorrhage can occur internally, with some lesions potentially forming cavities. Calcification is infrequently noted. Enhanced CT scans frequently reveal uneven ring-shaped enhancement or thick ring-shaped enhancement surrounding the tumor, resembling a "pseudocapsule". The central region typically demonstrates either subtle enhancement or patchy uneven enhancement. The pathological basis for these imaging characteristics primarily involves lung cancer tissue rich in blood supply surrounding the lesion, while the central area predominantly consists of sarcoma components that have poor vascularization. Mucinous degeneration along with necrosis or hemorrhage is also likely to occur [14,15]. The annular enhancement coupled with an irregular low-density area at the center following enhanced CT scanning exhibits distinctive features; however, the presence of a pseudocapsule may lead to misdiagnosis as a benign mass or pulmonary tuberculosis. In this case study, plain chest CT revealed a mass located in the upper lobe of the right lung that was closely adherent to both the interlobar fissure and lateral pleural membrane; it exhibited clear edges but demonstrated uneven internal density. Upon contrast enhancement, this mass displayed irregular mild to moderate enhancement on its pleural aspect while showing no significant enhancement centrally and presenting with a pseudocapsule around it—consistent with prior literature reports.

PSC is characterized by its high invasiveness and a tendency for vascular invasion and early metastasis [5,10]. However, the clinical manifestations of PSC often lack specificity. In the initial stages, patients typically exhibit few or only mild subjective symptoms. Consequently, most individuals are diagnosed at an advanced stage when seeking medical attention. This delay can be attributed to factors such as the mass's location, lesion size, and extent of invasion. When PSC occurs in the hilar region, tumors tend to grow both intraluminally and extraluminally. These masses are generally large enough to compress and obstruct the bronchi, leading to complications such as obstructive pneumonia or atelectasis. Patients may experience clinical symptoms including cough, sputum production, hemoptysis, dyspnea, and fever. Additionally, lymphadenopathy in the hilar region and mediastinum is frequently observed.

In contrast, PSC located outside the hilar area often presents with minimal or no subjective symptoms initially. As tumor growth accelerates and invades surrounding pleural tissue, patients may develop chest pain along with other manifestations. Distant metastases are common in this scenario; potential sites include hilar and mediastinal lymph nodes as well as bones, brain tissue, lungs, gastrointestinal tract organs like liver and adrenal glands [16–18]. In this particular case study, imaging via chest CT revealed a mass adjacent to the lateral pleura. Postoperatively, within the surgical site, a mass re-emerged that invaded towards the chest wall. Notably, recurrence was documented just ten months following surgery. The patient died during the follow-up, suggesting that PSC is prone to recurrence after surgical resection, with a poor prognosis and a high mortality rate.

The measured lesion size in the preoperative CT image for this case was 5.8 cm $\times$ 5.2 cm $\times$ 5.0 cm, whereas the tumor size in the postoperative pathological specimen was recorded as 7.0 cm $\times$ 5.0 cm $\times$ 3.5 cm. The discrepancies between the estimated and actual tumor sizes may be attributed to several factors: a CT scan layer thickness of 5 mm may overlook certain details; additionally, the reconstruction algorithm could result in an incomplete representation of the tumor's edges or induce partial volume effects, thereby affecting accurate measurement of the maximum diameter of the tumor. Furthermore, tissue dehydration and contraction caused by postoperative specimen fixation can vary depending on tissue composition (such as proportions of fibrosis and necrosis). The high heterogeneity observed in PSC may further exacerbate contraction across different dimensions (for instance, a reduction from 5.0 cm to 3.0 cm might indicate dehydration-related contraction, while an increase from 5.8 cm to 7.0 cm could reflect tension release and restoration of original shape following tumor resection). Preoperative laboratory examination results indicated that the patient's white blood cell count was elevated to 15.8 $\times$ 10^9/L (normal range: 4–10 $\times$ 10^9/L), with neutrophils constituting approximately 74.6% (normal range: 50%–70%). Such significantly elevated white blood cell counts ($>$15 $\times$ 10^9/L) along with a neutrophil percentage exceeding $>$80%, combined with symptoms such as cough and expectoration, suggest a potential pulmonary infection. Moreover, CT imaging revealed right pleural effusion. Considering these findings alongside central necrosis within the tumor and evidence of pleural invasion, it is more likely to be malignant pleural effusion caused by tumor progression or necrosis.

Differential Diagnosis

PSC should be differentially diagnosed from benign lesions such as pulmonary abscess and tuberculosis, as well as other NSCLCs on CT imaging. Key distinguishing features include: (1) PSC typically demonstrates incomplete necrosis with ill-defined boundaries between necrotic and

non-necrotic areas, whereas pulmonary abscesses often exhibit complete necrosis surrounded by enhanced granulation tissue, manifesting as peripheral or septal enhancement with marked contrast effect. PSC generally shows minimal peripheral infiltration without satellite lesions, and any cavitation usually presents with mural nodules of uneven thickness. In contrast, pulmonary abscesses initially appear as consolidation, progressing to thick-walled cavities with prominent air-fluid levels surrounded by extensive exudative consolidation. Tuberculous cavities typically display smooth inner walls (either thin- or thick-walled) accompanied by peripheral micronodules and fibrous strands. (2) PSC commonly presents as a large, relatively well-circumscribed mass with heterogeneous density, frequent necrosis, and rare calcification. Contrast-enhanced scans reveal significant enhancement of tumor parenchyma with central irregular hypodense areas, resulting in irregular ring-like enhancement. Other NSCLCs generally exhibit irregular morphology, less frequently forming large round masses, and typically demonstrate lobulated margins, spiculation, pleural indentation, and vascular convergence. Their enhancement patterns usually show homogeneous enhancement or irregular linear/patchy enhancement.

Conclusions

In summary, PSC is a rare and highly malignant tumor exhibiting both carcinomatous and sarcomatous features, characterized by aggressive behavior, early metastasis, frequent recurrence, and poor prognosis. Its clinical manifestations and chest CT findings lack specificity, often leading to misdiagnosis as tuberculosis or inflammatory lesions in early stages and posing challenges in distinguishing it from other NSCLCs at advanced stages. For elderly male patients with a long-term heavy smoking history, CT findings of large pulmonary masses with relatively well-defined margins, heterogeneous density on plain scan, "pseudocapsule" enhancement patterns, and proximity to the pleura should raise suspicion for PSC. However, definitive diagnosis ultimately relies on pathological examination supplemented by immunohistochemical analysis to confirm its biphasic differentiation.

Availability of Data and Materials

The datasets used and/or analyzed during the current study are contained within the article.

Author Contributions

Conceptualization, LFX and PZ; investigation, XSZ; writing—original draft preparation, LFX and XSZ; writing—review and editing, LFX, XSZ and PZ; visualization, FC; supervision, FC and PZ. All authors have read and agreed to the published version of the manuscript. All authors have participated sufficiently in the work and agreed to be accountable for all aspects of the work.

Ethics Approval and Consent to Participate

This case report was conducted in compliance with the Declaration of Helsinki (2013). This study received an exemption from requiring written informed consent, granted by the Ethics Committee of the First People's Hospital of Tongxiang City (Approval No. AF/SS-08/01.0). This exemption aligns with institutional and international guidelines for retrospective case reports, which involve anonymized clinical observations without experimental intervention, thereby safeguarding patient confidentiality.

Acknowledgment

We thank all the individuals for their participation in this study.

Funding

This research received no external funding.

Conflict of Interest

The authors declare no conflict of interest.

Supplementary Material

Supplementary material associated with this article can be found, in the online version, at https://doi.org/10.24976/Discov.Med.202537197.100.

References

[1] Sun L, Dai J, Chen Y, Duan L, He W, Chen Q, *et al*. Pulmonary Sarcomatoid Carcinoma: Experience From SEER Database and Shanghai Pulmonary Hospital. The Annals of Thoracic Surgery. 2020; 110: 406–413. https://doi.org/10.1016/j.athoracsur.2020.02.071.

[2] Rossi G, Cavazza A, Sturm N, Migaldi M, Facciolongo N, Longo L, *et al*. Pulmonary carcinomas with pleomorphic, sarcomatoid, or sarcomatous elements: a clinicopathologic and immunohistochemical study of 75 cases. The American Journal of Surgical Pathology. 2003; 27: 311–324. https://doi.org/10.1097/00000478-200303000-00004.

[3] Soewondo W, Adzhani F, Hanafi M, Firdaus ZJ. Lung adenocarcinoma size as a predictor of distant metastasis: A CT scan-based measurement. Narra J. 2024; 4: e1024. https://doi.org/10.52225/narra.v4i2.1024.

[4] Guo X, Wang J, Li D, Wang B, Zhu H, Guo H. Case report: The outcomes of neoadjuvant immunotherapy combined with chemotherapy in pulmonary sarcomatoid carcinoma: case series and literature review. Frontiers in Immunology. 2024; 15: 1467755. https://doi.org/10.3389/fimmu.2024.1467755.

[5] Mansfield AS, Roden AC, Boland JM. Towards a Molecular Classification of Pulmonary Sarcomatoid Carcinomas. Journal of Thoracic Oncology. 2017; 12: 910–912. https://doi.org/10.1016/j.jtho.2017.04.012.

[6] Franks TJ, Galvin JR. Sarcomatoid carcinoma of the lung: histologic criteria and common lesions in the differential diagnosis. Archives of Pathology & Laboratory Medicine. 2010; 134: 49–54. https://doi.org/10.5858/2008-0547-RAR.1.

[7] Bondili SK, Nandhana R, Dhanawat A, Noronha V, Joshi A, Patil VM, *et al*. Characteristics and clinical outcomes of pulmonary sarcomatoid carcinoma: experience from Tata Memorial Centre. Ecancermedicalscience. 2022; 16: 1438. https://doi.org/10.3332/ecancer.2022.1438.

[8] Steuer CE, Behera M, Liu Y, Fu C, Gillespie TW, Saba NF, *et al*. Pulmonary Sarcomatoid Carcinoma: An Analysis of the National Cancer Data Base. Clinical Lung Cancer. 2017; 18: 286–292. https://doi.org/10.1016/j.cllc.2016.11.016.

[9] Nicholson AG, Tsao MS, Beasley MB, Borczuk AC, Brambilla E, Cooper WA, *et al*. The 2021 WHO Classification of Lung Tumors: Impact of Advances Since 2015. Journal of Thoracic Oncology. 2022; 17: 362–387. https://doi.org/10.1016/j.jtho.2021.11.003.

[10] Yvorel V, Patoir A, Casteillo F, Tissot C, Fournel P, Stachowicz ML, *et al*. PD-L1 expression in pleomorphic, spindle cell and giant cell carcinoma of the lung is related to TTF-1, p40 expression and might indicate a worse prognosis. PLoS ONE. 2017; 12: e0180346. https://doi.org/10.1371/journal.pone.0180346.

[11] Litzky LA. Pulmonary sarcomatous tumors. Archives of Pathology & Laboratory Medicine. 2008; 132: 1104–1117. https://doi.org/10.5858/2008-132-1104-PST.

[12] Zuo L, You H, Cai Z, Liao S, Lu X, Li L, *et al*. Melan-A expression in non-melanocytic carcinoma: A potential diagnostic pitfall. Histology and Histopathology. 2024; 39: 1037–1041. https://doi.org/10.14670/HH-18-696.

[13] Jakobsen JN, Sørensen JB. Clinical impact of ki-67 labeling index in non-small cell lung cancer. Lung Cancer. 2013; 79: 1–7. https://doi.org/10.1016/j.lungcan.2012.10.008.

[14] Tang W, Wen C, Pei Y, Wu Z, Zhong J, Peng J, *et al*. Preoperative CT findings and prognosis of pulmonary sarcomatoid carcinoma: comparison with conventional NSCLC of similar tumor size. BMC Medical Imaging. 2023; 23: 105. https://doi.org/10.1186/s12880-023-01065-8.

[15] Sihag S. Commentary: Sarcomas and sarcomatoid tumors of the lung…not your average lung cancers. The Journal of Thoracic and Cardiovascular Surgery. 2021; 162: 285–286. https://doi.org/10.1016/j.jtcvs.2020.04.082.

[16] Gu L, Xu Y, Chen Z, Pan Y, Lu S. Clinical analysis of 95 cases of pulmonary sarcomatoid carcinoma. Biomedicine & Pharmacotherapy. 2015; 76: 134–140. https://doi.org/10.1016/j.biopha.2015.10.009.

[17] Ito K, Oizumi S, Fukumoto S, Harada M, Ishida T, Fujita Y, *et al*. Clinical characteristics of pleomorphic carcinoma of the lung. Lung Cancer. 2010; 68: 204–210. https://doi.org/10.1016/j.lungcan.2009.06.002.

[18] Taira N, Kawabata T, Ichi T, Kushi K, Yohena T, Kawasaki H, *et al*. A case of synchronous double primary lung cancer presenting with pleomorphic carcinoma and adenocarcinoma. The American Journal of Case Reports. 2014; 15: 576–579. https://doi.org/10.12659/AJCR.892339.